Electronic Supplementary Material (ESI) for Inorganic Chemistry Frontiers.
This journal is © the Partner Organisations 2022

Electronic Supplementary Information

Experimental Section

Materials: TM was provided by Suzhou Taili New Energy Co., Ltd. NaOH, Na_2SO_4, NH_4Cl, $Co(NO_3)_2·6H_2O$, NH_4F, $CO(NH_2)_2$, $C_7H_6O_3$, $C_6H_5Na_3O_7·2H_2O$, $C_9H_{11}NO$, $Na_2Fe(CN)_5NO·2H_2O$, NaH_2PO_2, and NaClO were purchased from Aladdin Ltd. (Shanghai, China). H_2O_2, H_2SO_4, HCl, $N_2H_4·H_2O$, and C_2H_5OH were purchased from Beijing Chemical Corp. (China). A mixed gas of NO/Ar (10 *vol.*% NO) was purchased from Yinde City Xizhou Gas Co., Ltd (China). The water used in this work was purified through a Millipore system. All reagents were analytical reagent grade without further purification.

Preparation of CoP/TM: To synthesize CoP/TM, its hydroxide nanoarray precursor was prepared firstly via a hydrothermal method. By dissolving $Co(NO_3)_2·6H_2O$ (0.485 g), NH_4F (0.155 g), and $CO(NH_2)_2$ (0.500 g) in 35 mL of ultrapure water and stirring for 0.5 h, an aqueous solution can be obtained. Then, pretreated TM (cleaned firstly by HCl, ethanol, and ultrapure water, 2 cm × 3 cm) were transferred into this solution, which were together sealed in an autoclave and maintained at 120 °C for 6 h. The as-fabricated Co(OH)F/TM was cleaned with water and air dried. Then, it was placed in a tube furnace with another 1 g of NaH_2PO_2 at the upstream position. With only 2 h of heating treatment at 300 °C under argon atmosphere (99.999%), the self-supported CoP/TM can be obtained (loading: ~2.0 mg cm^{-2}).

Characterizations: XRD data were acquired on a Shimadzu XRD-6100 diffractometer with Cu Kα radiation (40 kV, 30 mA) of wavelength 0.154 nm. SEM and EDX elemental mapping images were collected on a Gemini SEM 300 scanning electron microscope (ZEISS, Germany) at an accelerating voltage of 5 kV. XPS measurements were performed on an ESCALABMK II X-ray photoelectron spectrometer using Mg as the exciting source. Absorbance data were acquired on SHIMADZU UV-2700 UV-Vis spectrophotometer. Gas chromatography analysis was performed on GC-2014C (Shimadzu Co.) with thermal conductivity detector and

nitrogen carrier gas.

Electrochemical measurements: Electrochemistry NORR tests were carried out in 0.2 M Na_2SO_4 solution (pH = 7) using a typical H-cell separated by a clean piece of Nafion 117 membrane under ambient conditions (using CHI 660E electrochemical analyzer). We used NO/Ar mixed gas with a low NO content (10 *vol.*%) as inlet gas. The gas flow rate was controlled by the mass flow controllers (Beijing Sevenstar Electronics Co., Ltd.). The membrane was protonated with boiled water, H_2O_2 (5%) solution, as well as 0.5 M H_2SO_4, successively. The electrochemical experiments were carried out with a three-electrode configuration using CoP/TM with a cutting size of 0.25 cm^2 as working electrodes, a platinum foil (4 cm^2) as the counter electrode, and a standard Ag/AgCl as the reference electrode. In all measurements, saturated Ag/AgCl electrode was calibrated to RHE if there are no special notes as following: E (RHE) = E (Ag/AgCl) + 0.059 × pH + 0.197 V. LSV was conducted at a scan rate of 5 mV s^{-1} with iR correction. Before each measurement, Ar gas (purity: 99.99%) was purged into the solution for at least 30 min to remove residual air in the reservoir. Controlled potential electrolysis was then performed at each potential for 1 h. For consecutive cycle stability tests, potentiostatic electrolysis was performed at the optimal potential (−0.2 V in this work) for 1 h. After electrolysis, the electrolyte was analyzed by UV–Vis spectrophotometry. Then, potentiostatic tests were carried out under the same conditions using the fresh electrolyte for the next cycle without changing the working electrode to confirm the electrochemical reusability of the catalyst. Thus, in this work, each "cycle" represents a 1-h bulk electrolysis test at −0.2 V under ambient conditions. ECSA was measured by CV at the potential window from 0.21 to 0.31 V versus Ag/AgCl, with different scan rates of 10, 20, 30, 40, 50, 60, 70, 80, 90 and 100 mV s^{-1}. The double-layer capacitance (C_{dl}) was estimated by plotting the $\Delta j = (j_a - j_c)$ at 0.26 V versus Ag/AgCl against the scan rates, in which the j_a and j_c were the anodic and cathodic current density, respectively. The slope is twice that of the C_{dl} values. C_{dl} was used to represent the ECSA. All the above

measurements were at room temperature under atmospheric pressure and carried out without ohmic-drop correction unless noted otherwise. The area of the working electrode in the electrolyte was controlled at 0.25 cm^2, and all current densities were normalized to the geometrical area of the electrode.

Determination of NH_3: The amount of NH_3 in the solution was determined by colorimetry using the indophenol blue method. A certain amount of electrolyte was taken out from the electrolytic cell and diluted to 2 mL to the detection range. Then, 2 mL of 1 M NaOH solution that contains salicylic acid and sodium citrate was added. Then, 1 mL of 0.05 M NaClO and 0.2 mL of 1 wt% $C_5FeN_6Na_2O{\cdot}2H_2O$ were added to the above solution. After standing at room temperature for 2 h, the UV-Vis absorption spectrum was measured. The concentration of NH_3 was determined using the absorbance at a wavelength of 660 nm. The concentration-absorbance curve was calibrated using a series of standard NH_4Cl solutions. Fitting curve ($y = 0.449x + 0.0382$, $R^2 = 0.9999$, showing good linear relation) are calculated and plotted in the supporting information.

Determination of N_2H_4: The N_2H_4 presented in the electrolyte was estimated by Watt and Chrisp method. Color reagent includes $C_9H_{11}NO$ (5.99 g), HCl (concentrated, 30 mL) and ethanol (300 mL). 1 mL above color reagent and 1 mL electrolyte were mixed and stirred 15 min at room temperature. The concentration of N_2H_4 was determined using the absorbance at a wavelength of 455 nm. The absorbance curves were calibrated using standard N_2H_4 solution with a series of concentrations. The fitting curve ($y = 0.731x+0.156$, $R^2 = 0.9993$) is provided in the supporting information.

Determination of H_2 and N_2: The gas product (H_2 and N_2) was monitored by GC.

Determination of NH_3 FE and yield:

The FE for NH_3 electrosynthesis was defined as the amount of electric charge used for producing NH_3 divided by the total charge passed through the electrodes during the electrolysis. The FE was calculated according to the following equation:

$$FE = n \times F \times c \times V / (M \times Q) \quad (1)$$

The NH_3 yield was calculated using the following equation:

$$NH_3 \text{ yield} = c_{NH3} \times V / (17 \times t \times S) \quad (2)$$

Where n is the number of electrons was needed to produce one product molecule, F is Faradic constant (96485 C mol^{-1}); c is the measured mass concentration of product; V is the volume of the cathodic reaction electrolyte (30 mL); M is relative molecular mass of specific product; Q is the quantity of applied charge/electricity; t is the time for which the potential was applied (1 h); S is the geometric area of the working electrode (0.25 cm^2).

Zn–NO battery: CoP/TM was employed as the cathode to perform the NORR in a cathodic electrolyte (0.2 M Na_2SO_4). A polished Zn plate (purity：>99.999%, ~¥300 for 0.2mm×0.2m×10m) was set in an anodic electrolyte (1 M KOH), and a bipolar membrane was used to separate the two different electrolytes. Zn–NO battery potentially has a higher voltage output than those of the O_2–based batteris (as displayed in Table S3). During the battery discharge process, electrochemical NO reduction occurs on CoP/TM, and Zn converts to ZnO. The electrochemical reactions on each electrode can be described as follows:

$$\text{Cathode: } NO + 5H^+ + 5e^- \rightarrow NH_3 + H_2O \quad (3)$$

$$\text{Anode: } Zn + 2OH^- \rightarrow ZnO + H_2O + 2e^- \quad (4)$$

$$\text{Overall: } 5Zn + 2NO + 3H_2O \rightarrow 5ZnO + 2NH_3 \quad (5)$$

Computational details: All calculations were performed using Vienna Ab Initio Simulation Package (VASP) with the spin-polarized density functional theory (DFT) method employed. Taking into account the vander Waals interactions, a DFT-D3 semiempirical scheme was applied. The projector-augmented-wave (PAW) method was used to describe the ion−electron interactions, and the Perdew−Burke−Ernzerhof (PBE) and generalized gradient approximation (GGA) were chosen for the

exchange−correlation functional to treat the interactions between electrons. The plane wave cutoff energy was set to 450 eV. The convergence threshold for energy and force was respectively 10^{-5} eV and 0.02 eV $Å^{-1}$. The Brillouin zone is sampled with a Monkhorst−Pack grid of 3 × 3 × 1. A vacuum space over 15 Å is employed to avoid the interaction between adjacent units.

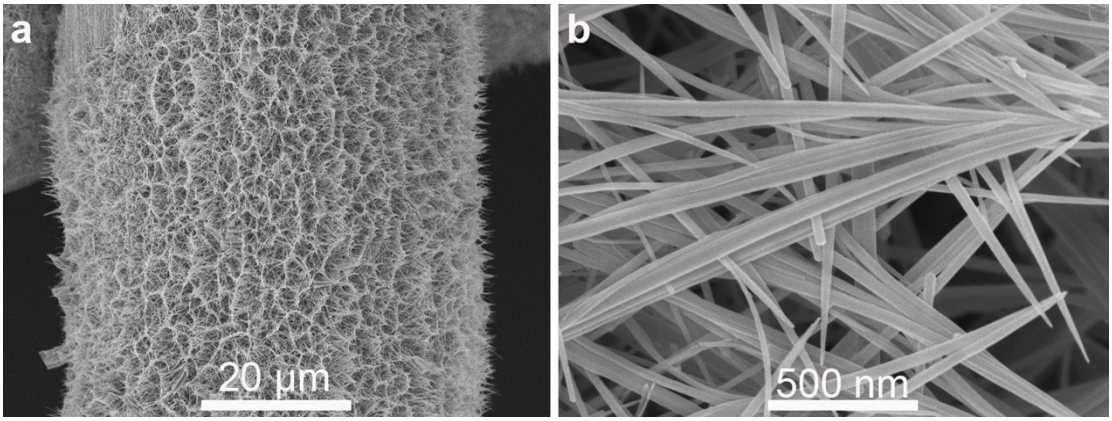

Fig. S1. SEM images of the Co(OH)F/TM precursor.

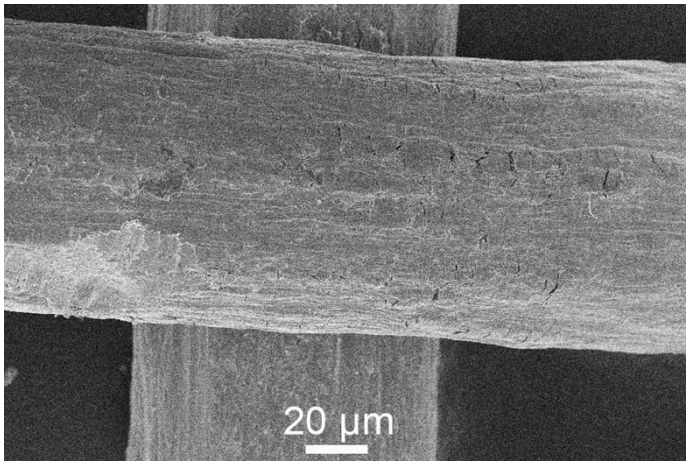

Fig. S2. SEM image of bare TM.

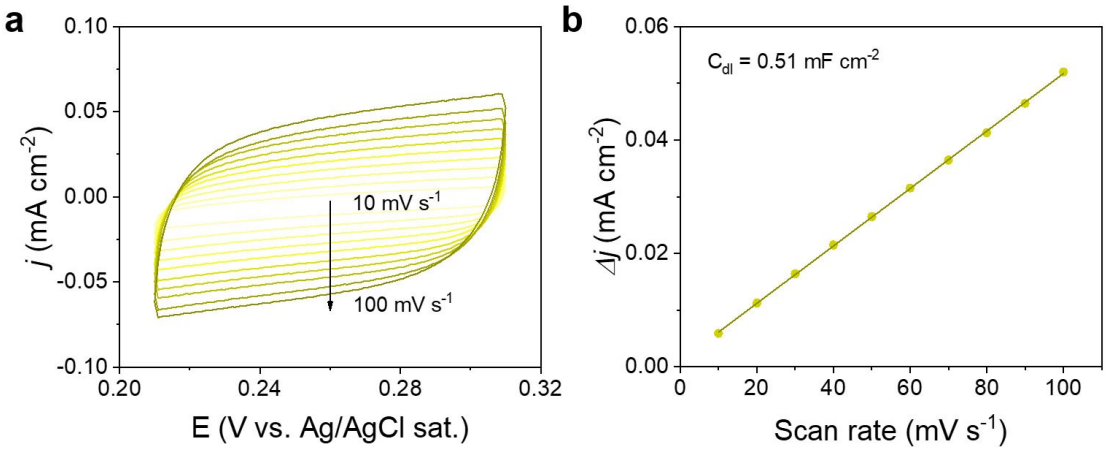

Fig. S3. (a) Cyclic voltammograms for Co(OH)F/TM in the double layer region at different scan rates of 10, 20, 30, 40, 50, 60, 70, 80, 90, and 100 mV s^{-1} in 0.2 M Na_2SO_4 electrolyte. (b) Capacitive current densities as a function of scan rates for Co(OH)F/TM.

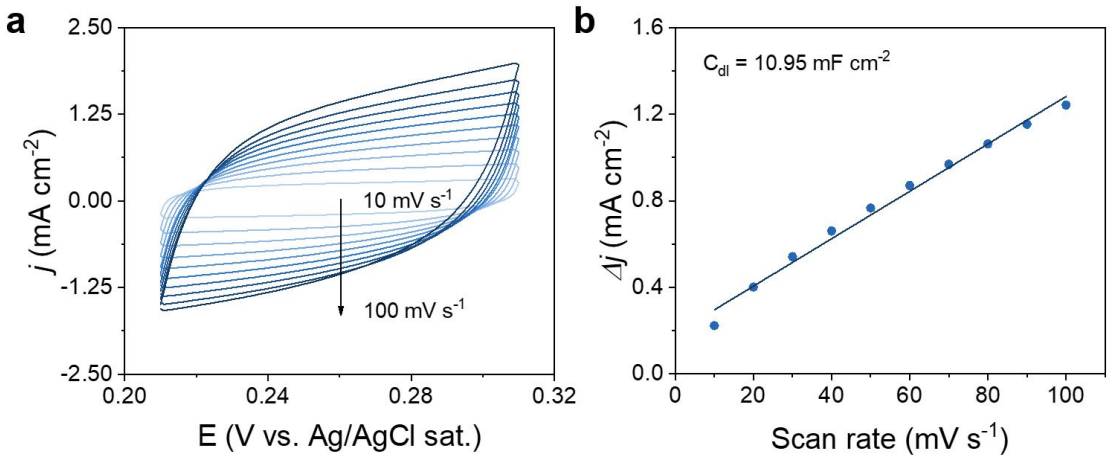

Fig. S4. (a) Cyclic voltammograms for CoP/TM in the double layer region at different scan rates of 10, 20, 30, 40, 50, 60, 70, 80, 90, and 100 mV s^{-1} in 0.2 M Na_2SO_4 electrolyte. (b) Capacitive current densities as a function of scan rates for CoP/TM.

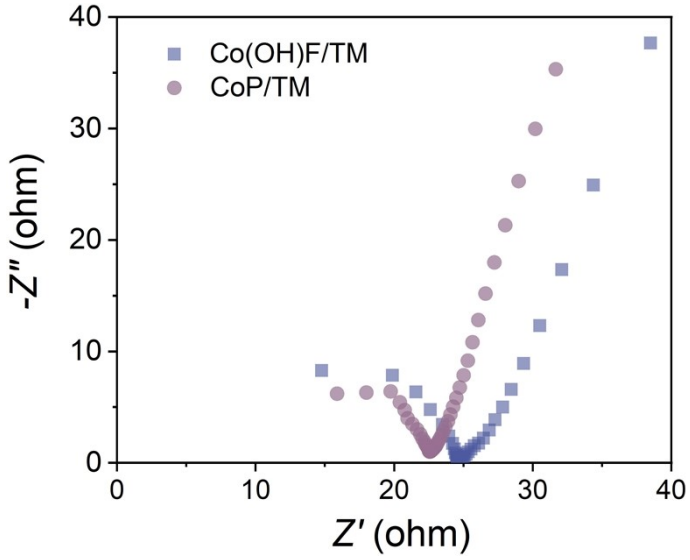

Fig. S5. Electrochemical impedance spectroscopy measurements of Co(OH)F/TM and CoP/TM.

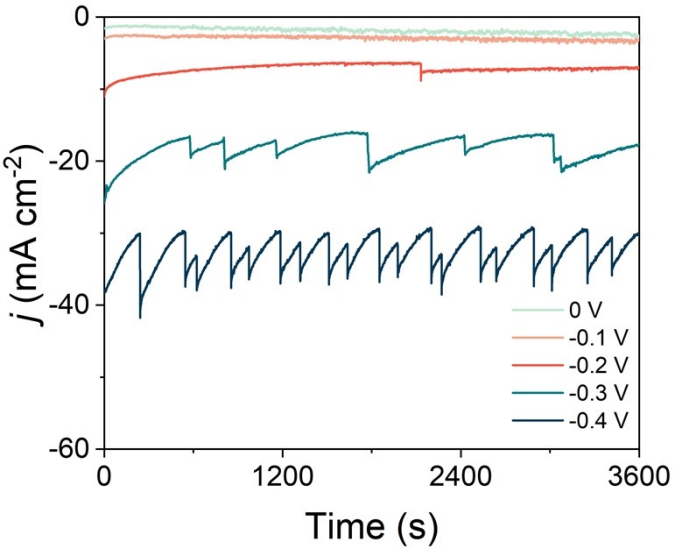

Fig. S6. Chronoamperometry tests at various applied potentials in NO-saturated 0.2 M Na_2SO_4 for CoP/TM.

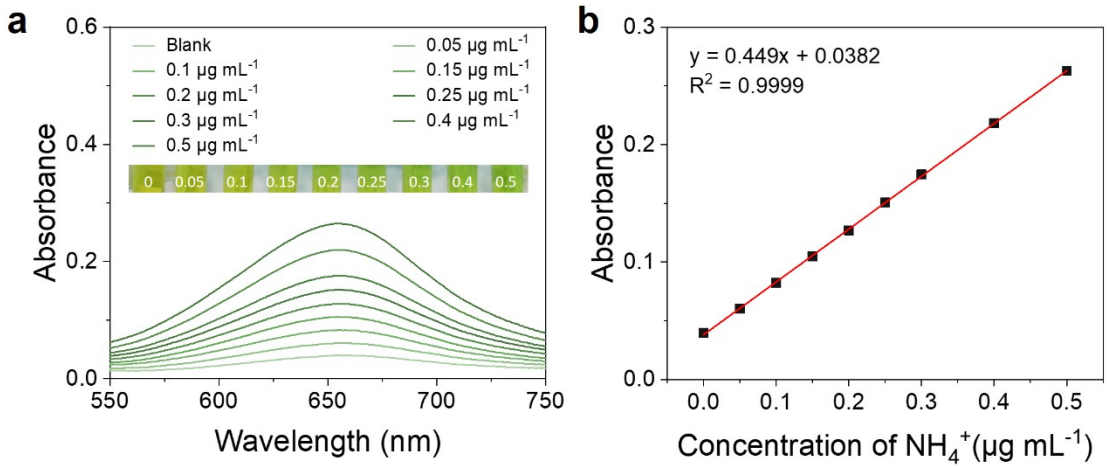

Fig. S7. (a) UV-Vis absorption spectra of indophenol assays with NH_3 after incubated for 2 h at room temperature and corresponding (b) calibration curve used for estimating NH_3.

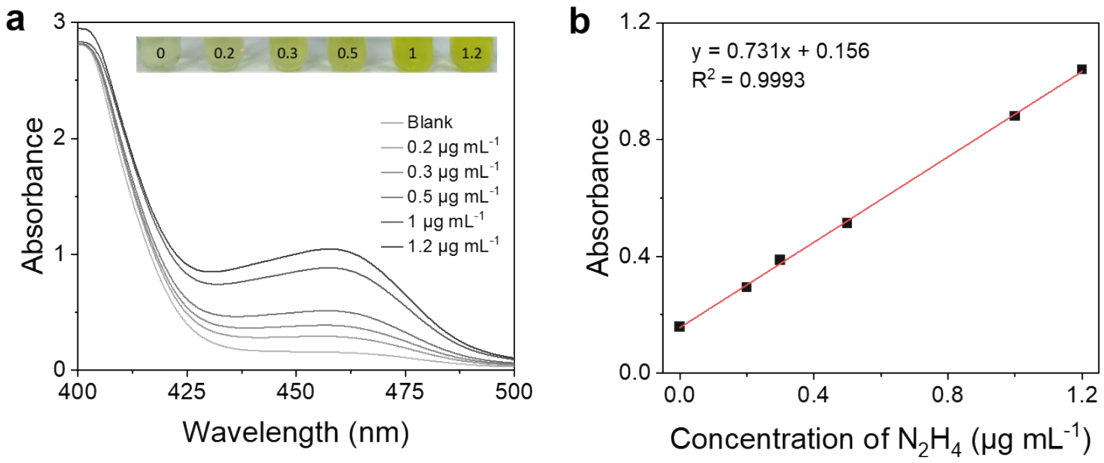

Fig. S8. (a) UV-Vis absorption spectra of various N_2H_4 concentration after incubated for 15 min at room temperature and corresponding (b) calibration curve used for estimating N_2H_4.

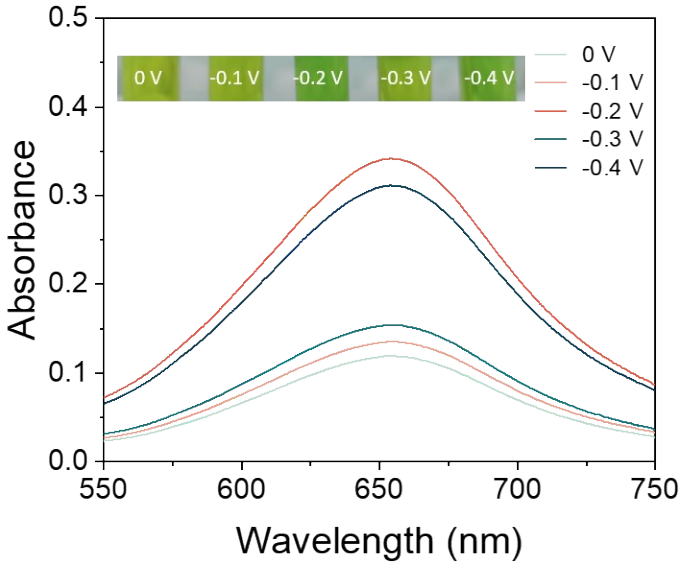

Fig. S9. UV-Vis absorption spectra of the electrolytes stained with indophenol indicator after 1 h electrolysis on CoP/TM at various applied potentials.

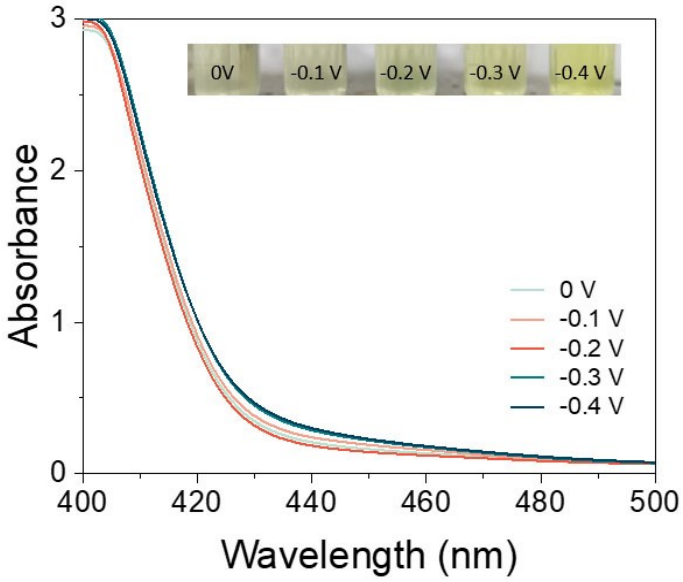

Fig. S10. UV-Vis absorption spectra of electrolytes estimated by the method of Watt and Chrisp after 1 h electrolysis on CoP/TM at each given potential.

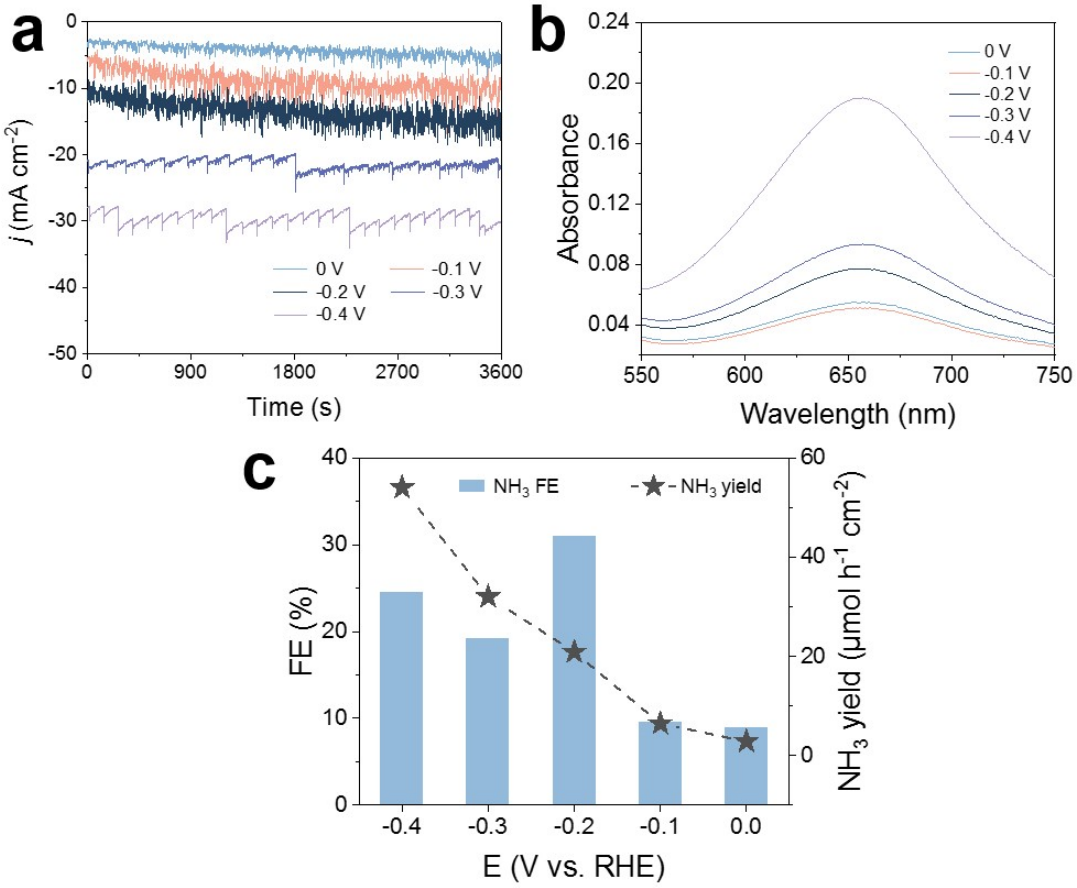

Fig. S11. NORR performance of CoP/TM in acidic media. (a) Chronoamperometry tests at various electrode potentials in NO-saturated 0.1 M HCl. (b) Corresponding UV-Vis spectra of the electrolytes colored with indophenol blue reagent. (c) NH_3 FEs and yields at different potentials.

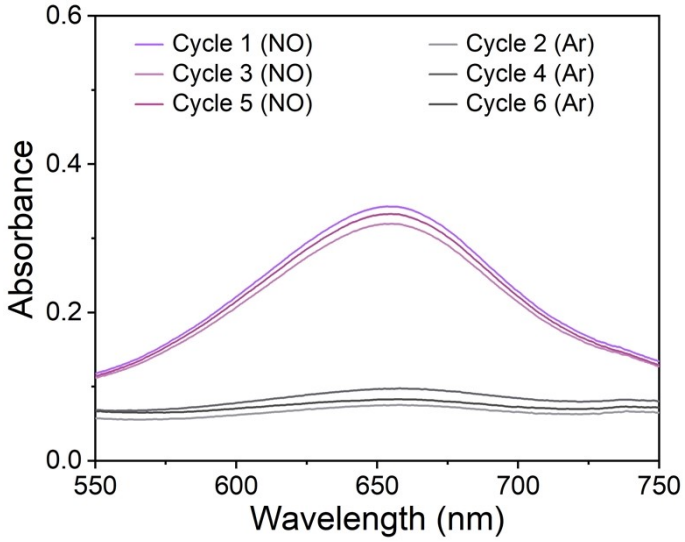

Fig. S12. UV-Vis spectra of the electrolytes colored with indophenol blue reagent for the alternating electrolysis test.

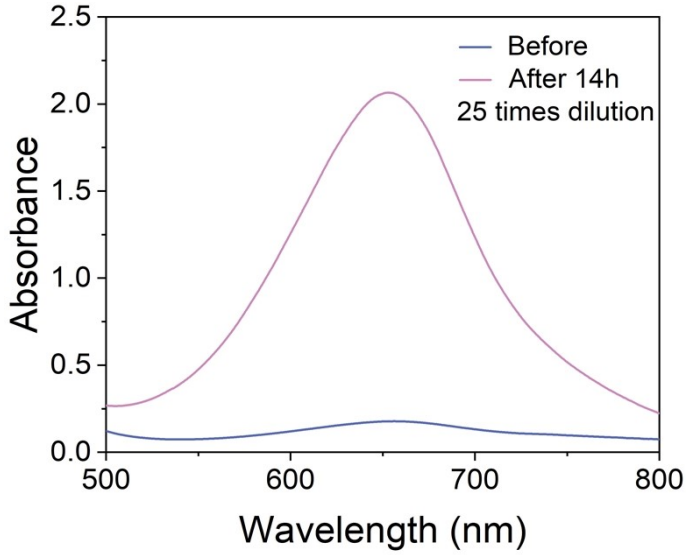

Fig. S13. UV-Vis absorption spectra of the electrolytes stained with indophenol indicator after 14 h electrolysis on CoP/TM at –0.2 V.

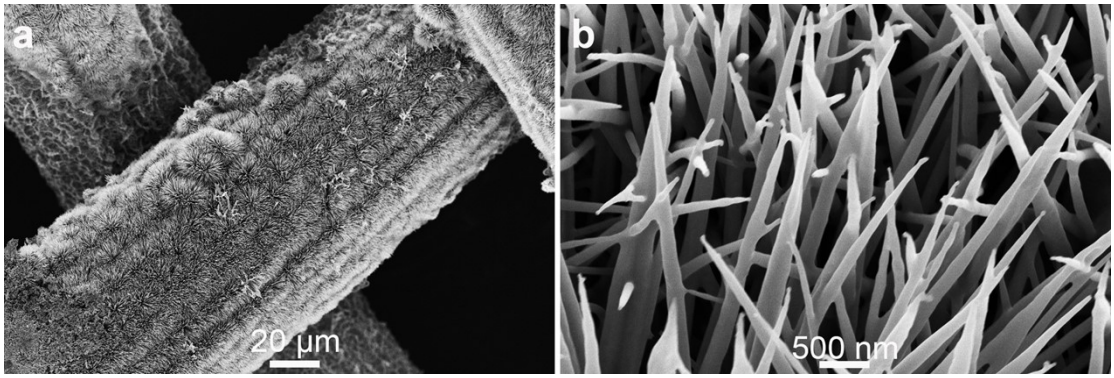

Fig. S14. SEM images for CoP/TM after stability test.

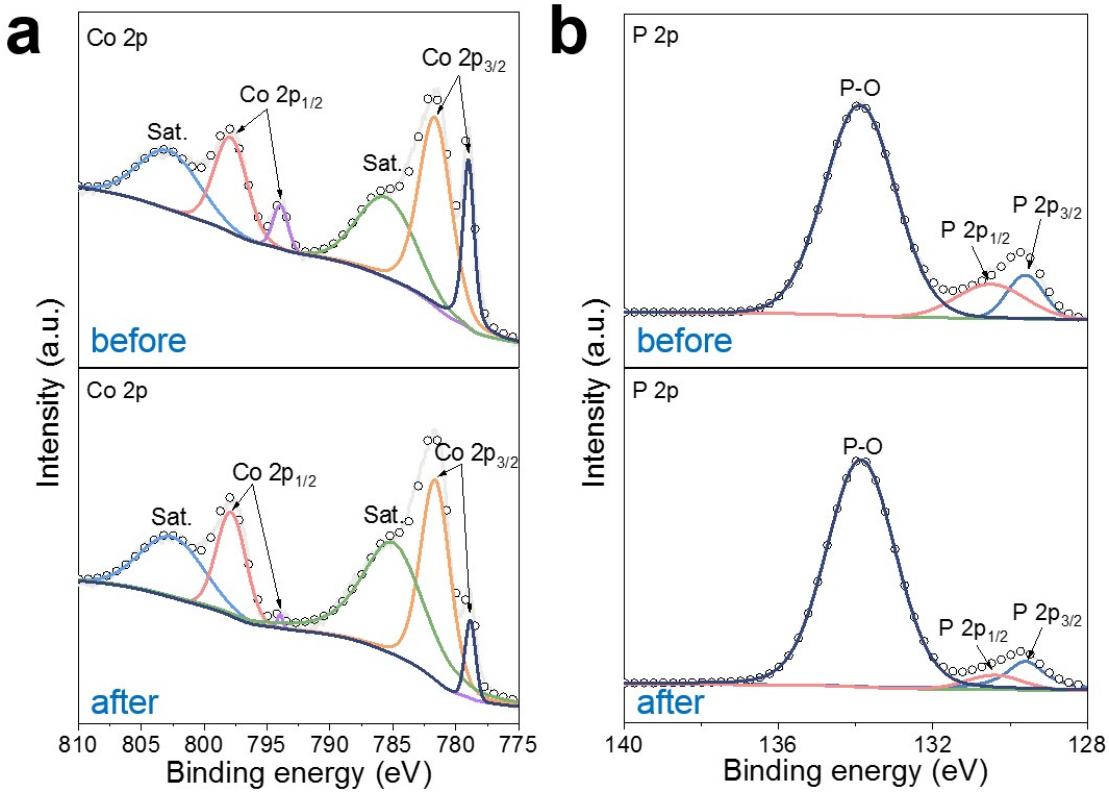

Fig. S15. XPS spectra of CoP/TM in the (a) Co 2p and (b) P 2p regions before and after the stability tests.

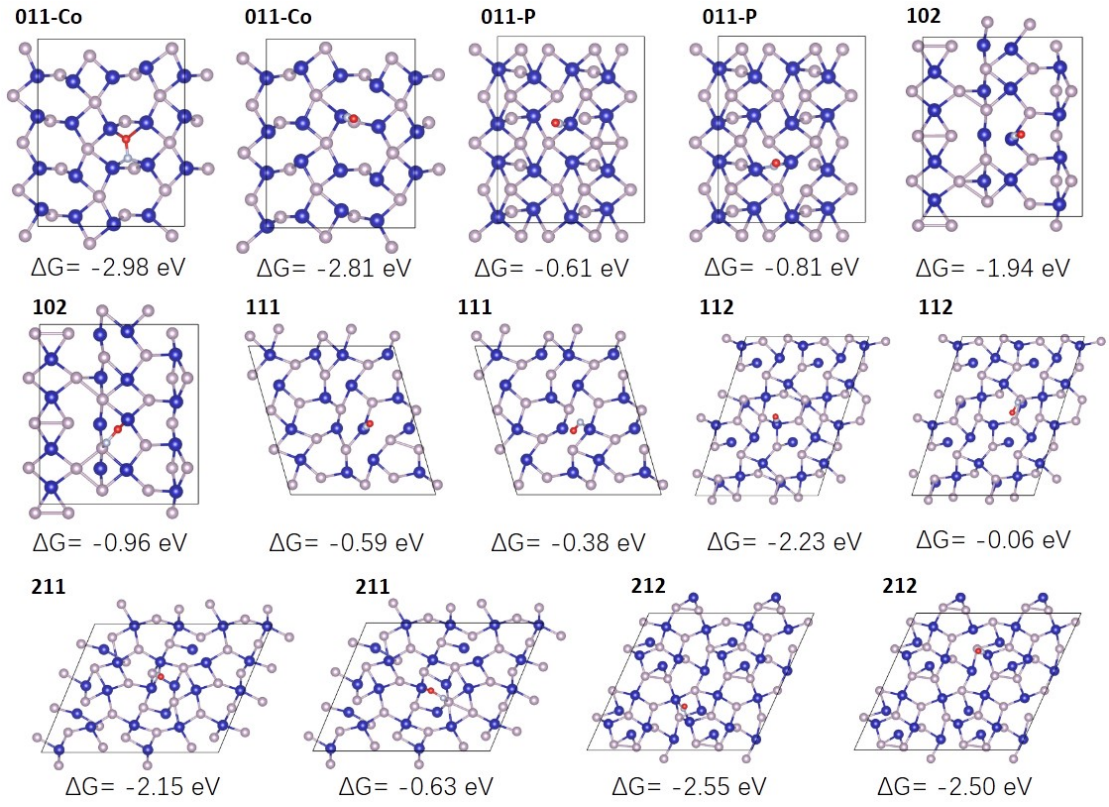

Fig. S16. Adsorption configurations on all possible crystal planes. Dark blue, purple, light blue, red, and pink spheres represent Co, P, N, O, and H atoms, respectively.

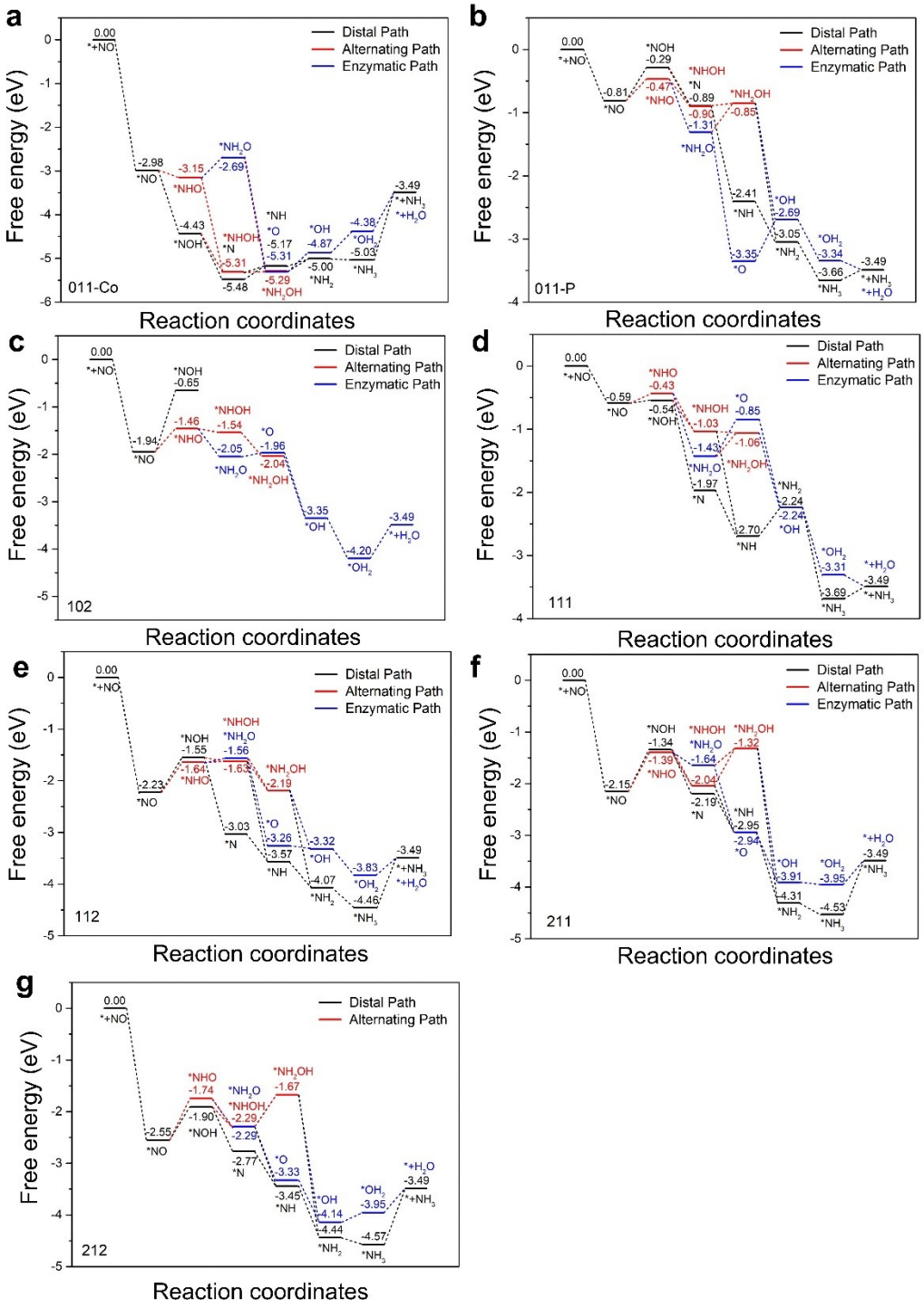

Fig. S17. Gibbs free energy diagrams of NORR on different crystal surfaces including (a) (011Co), (b) (011P), (c) (102), (d) (111), (e) (112), (f) (211), (g) (212) of CoP.

Table S1. Comparison of E_{onset}, NH_3 yield, and FE of the CoP/TM with recently reported aqueous-based NORR electrocatalysts.

Catalyst	Electrolyte	Purity of NO inlet gas	Feeding rate (sccm)	Testing cell system	E_{onset} (V *vs.* RHE)	NH_3 yield (μmol h^{-1} cm^{-2})	FE (%)	Ref.
CoP/TM	**0.2 M Na_2SO_4**	**10 *vol*.% NO**	**30**	**H-type cell**	**−0.012**	**47.22**	**88.3**	**This work**
MnO_{2-x} NA/TM	0.2 M Na_2SO_4	10 *vol*.% NO	30	H-type cell	−0.9	9.9	82.8	*Mater. Today Phys.*, 2022, **22** 100586
NiO/TM	0.1 M Na_2SO_4 + 0.5 mM Fe(II)EDTA	10 *vol*.% NO	30	H-type cell	−0.35	125.29	90	*Chem. Commun.*, 2021, **57**, 13562–13565
Ni_2P/CP	0.1 M HCl	10 *vol*.% NO	30	H-type cell	−0.12	33.47	76.9	*J. Mater. Chem. A*, 2021, **9**, 24268–24275
MoS_2/GF	0.1 M HCl + 0.5 mM Fe(II)SB	10 *vol*.% NO	30	H-type cell	0.45	99.6	76.6	*Angew. Chem. Int. Ed.*, 2021, **60**, 25263–25268
FeNC	0.1 M $HClO_4$	10 *vol*.% NO	60	three-electrode glass cell	0.12	~20.2	~5.1	*Nat. Commun.*, 2021, **12**, 1856
$Ru_{0.05}Cu_{0.95}$	0.5 M Na_2SO_4	1/4 (n/n)	50	H-type cell	−0.43	17.68	64.9	*Sci. China. Chem.*, 2021, **64**, 1493–1497
Single atom Nb	0.1 M HCl	/	20	three-channel flow cell	−0.15	295.2	77	*Nano Energy*, 2020, **78**, 105321
Cu foam	0.25 M Li_2SO_4	/	30	H-type cell	0.75	517.1	93.5	*Angew. Chem. Int. Ed.*, 2020, **59**, 9711–9718
Cu foil	0.25 M Li_2SO_4	/	30	H-type cell	0.5	95.0	/	
Pt foil	0.25 M Li_2SO_4	/	30	H-type cell	0.5	99.4	/	
$CoSe_2$@CNTs	Na_2SO_4 + Fe(II)EDTA	/	30	H-type cell	/	/	48.14	*Environ. Sci. Pollut. Res.*, 2017, **24**, 14249–14258

Table S2. Comparison of NH_3 yield and power density of our battery with recently reported metal–NO and metal–N_2 battery systems.

Catalyst	NH_3 yield	Power density (mW cm^{-2})	Ref.
CoP/TM	**284.99 μg h^{-1} $mg_{cat.}^{-1}$ (569.98 μg h^{-1} cm^{-2})**	**0.49647**	**This work**
NiO/CP	228 μg h^{-1} cm^{-2}	0.88	*Chem. Commun.*, 2021, **57**, 13562–13565
Ni_2P/CP	62.05 μg h^{-1} $mg_{cat.}^{-1}$ (43.44 μg h^{-1} cm^{-2})	1.53	*J. Mater. Chem. A*, 2021, **9**, 24268–24275
MoS_2/GF	411.8 μg h^{-1} $mg_{cat.}^{-1}$ (411.8 μg h^{-1} cm^{-2})	1.04	*Angew. Chem. Int. Ed.*, 2021, **60**, 25263–25268
Fe 1.0 HTNs	0.172 μg h^{-1} cm^{-2}	0.02765	*J. Mater. Chem. A*, 2021, **9**, 4026−4035
CoPi/HSNPC	11.62 μg h^{-1} $mg_{cat.}^{-1}$	0.31	*J. Mater. Chem. A*, 2021, **9**, 11370−11380
VN@NSC-900	0.172 μg h^{-1} cm^{-2}	0.01642	*Appl. Catal. B: Environ.*, 2021, **280**, 119434
CoPi/NPCS	14.7 μg h^{-1} $mg_{cat.}^{-1}$	0.49	*ACS Appl. Mater. Interfaces*, 2021, **13**, 12106−12117
NbS_2	/	0.31	*Appl. Catal. B: Environ.*, 2020, **270**, 118892
Graphene/Pd	27.1 mg h^{-1} $g_{cat.}^{-1}$	/	*Energy Environ. Sci.*, 2020, **13**, 2888−2895
BNFC-800	/	127	*J. Mater. Chem. A*, 2020, **8**, 8430−8439
Cu-2	0.125 μg h^{-1} cm^{-2}	0.0101	*Chem. Commun.*, 2019, **55**, 12801−12804

Table S3. Theoretical voltages for several types of metal-based batteries.

Battery type	Chemical reaction	Theoretical voltage (V)
Zn–NO	$5Zn + 2NO + 3H_2O \rightarrow 5ZnO + 2NH_3$	2.14
Li–S	$2Li + S \rightarrow Li_2S$	2.2
Li–O_2	$2Li + O_2 \rightarrow Li_2O_2$	3.0
Li–CO_2	$4Li + 3CO_2 \rightarrow C + 2Li_2CO_3$	2.7
Li–N_2	$6Li + N_2 \rightarrow 2Li_3N$	0.54
Zn–CO_2	$Zn + CO_2 + H_2O \rightarrow ZnO + HCOOH$	0.955
Al–N_2	$2Al + N_2 \rightarrow 2AlN$	0.99
Zn–Air	$2Zn + O_2 \rightarrow 2ZnO$	1.65
Zn–Nitrate	$4Zn + NO_3^- + 3H_2O \rightarrow 4ZnO + NH_4OH + OH^-$	1.85

Table S4. Gibbs free energy change ΔG_{*NO} of NO on each crystal surface.

		Adsorption configuration	***E*/eV**	E_{ZPE}	**∫CpdT**	**TS**	***G***	
		NO	**−12.29**	**0.12**	**0.10**	**0.65**	**−12.73**	
Crystal plane	***E*/eV**		***E*/eV**	**Thermal correction to *G*(*T*)**				ΔG_{*NO}/eV
011Co	−412.63	CoNO	−428.50	0.16			−428.34	−2.98
		CoNO	−428.32	0.16			−428.16	−2.81
011P	−428.98	CoNO	−442.46	0.14			−442.32	−0.61
		CoNO	−442.65	0.13			−442.51	−0.81
102	−812.57	CoNO	−827.36	0.12			−827.24	−1.94
		P-NO-Co	−826.39	0.13			−826.26	−0.96
111	−588.41	CoNO	−601.89	0.16			−601.73	−0.59
		CoNO	−601.62	0.10			−601.52	−0.38
112	−633.24	CoNO	−648.31	0.12			−648.19	−2.23
		PNO	−646.11	0.08			−646.03	−0.06
211	−637.56	CoNO	−652.60	0.16			−652.44	−2.15
		PNCoO	−651.05	0.13			−650.92	−0.63
212	−851.10	CoNO	−866.53	0.15			−866.38	−2.55
		CoNO	−866.44	0.12			−866.33	−2.50